

Formation of a narrow baryon resonance with positive strangeness in K^+ collisions with Xe nuclei

DIANA Collaboration

V.V. Barmin^a, A.E. Asratyan^a, V.S. Borisov^a, C. Curceanu^b,
 G.V. Davidenko^a, A.G. Dolgolenko^{a,*}, C. Guaraldo^b, M.A. Kubantsev^a,
 I.F. Larin^a, V.A. Matveev^a, V.A. Shebanov^a, N.N. Shishov^a,
 L.I. Sokolov^a, G.K. Tumanov^a, and V.S. Verebryusov^a

^a *Institute of Theoretical and Experimental Physics, Moscow 117259, Russia*

^b *Laboratori Nazionali di Frascati dell' INFN, C.P. 13-I-00044 Frascati, Italy*

May 28, 2018

Abstract

The data on the charge-exchange reaction $K^+Xe \rightarrow K^0pXe'$, obtained with the bubble chamber DIANA, are reanalyzed using increased statistics and updated selections. Our previous evidence for formation of a narrow pK^0 resonance with mass near 1538 MeV is confirmed and reinforced. The statistical significance of the signal reaches some 8σ (6σ) when estimated as S/\sqrt{B} ($S/\sqrt{B+S}$). The mass and intrinsic width of the Θ^+ baryon are measured as $m = 1538 \pm 2$ MeV and $\Gamma = 0.39 \pm 0.10$ MeV.

*Corresponding author. E-mail address: dolgolenko@itep.ru.

The baryons built of four quarks and an antiquark as the lowest Fock component, referred to as pentaquarks, are not forbidden by theory and have been discussed for many years [1]. Some properties of light pentaquark baryons forming the lowest $SU(3)$ multiplet, the antidecuplet, have been predicted by Diakonov, Petrov, and Polyakov in the framework of the chiral quark–soliton model [2]. In particular, they predicted $m \simeq 1530$ MeV and $\Gamma < 15$ MeV for the mass and width of the explicitly exotic baryon with positive strangeness, the $\Theta^+(uudd\bar{s})$ that should decay to the nK^+ and pK^0 final states. More recent theoretical analyses suggest that the Θ^+ intrinsic width may be as small as ~ 1 MeV or even less [3]. Narrow peaks near 1540 MeV in the nK^+ and pK^0 mass spectra were initially detected in low-energy photoproduction [4] and in the charge-exchange reaction $K^+n \rightarrow pK^0$ [5]. Subsequently, both experiments were able to confirm their initial observations [6, 7]. Moreover, increasing the statistics of the charge-exchange reaction allowed DIANA to directly estimate the Θ^+ intrinsic width: $\Gamma = 0.36 \pm 0.11$ MeV [7]. Other searches for the Θ^+ baryon in different reactions and experimental conditions yielded both positive and negative results, see the review papers [8] and [9] and references therein. The bulk of null results can be probably explained by the extreme smallness of the Θ^+ width that implies the smallness of production cross-sections [10].

The charge-exchange reaction $K^+n \rightarrow K^0p$ on a bound neutron, that is investigated by DIANA and BELLE [11], is particularly interesting because it allows to probe the Θ^+ intrinsic width in a model-independent manner. The existing data on low-energy K^+D scattering have been found to leave room for a pK^0 resonance with mass near 1540 MeV, provided that its width is less than 1 MeV [12, 13, 14, 15, 16]. An important advantage of the reaction $K^+n \rightarrow K^0p$ is that the strangeness of the final-state pK_S^0 system is *a priori* known to be positive. In this paper, the DIANA data on the charge-exchange reaction $K^+Xe \rightarrow K^0pXe'$ are reanalyzed using increased statistics and updated selections.

The detector and the experimental procedure have been detailed in [7] and references therein. Briefly, the non-magnetic bubble chamber DIANA was filled with liquid Xenon and exposed to a separated K^+ beam with $p = 850$ MeV from the 10-GeV proton synchrotron at ITEP, Moscow. A K^+ traveling through the chamber volume is continuously decelerated by ionization, and its momentum at collision point is a tabulated function of its path in liquid Xenon. Thereby, we are able to scan K^+Xe collisions over an extended interval of K^+ momentum between zero and some 700 MeV. On the other hand, soft charged secondaries are efficiently identified by bubble sensity and momentum-

analyzed by range in Xenon. (Note that this simple and elegant scheme will be imitated in future high-statistics studies of the charge-exchange reaction, see [17].) The estimate of K^+ momentum based on measured position of the interaction vertex has been verified by detecting and reconstructing the $K^+ \rightarrow \pi^+\pi^+\pi^-$ decays in flight.

Scanning of the film yielded nearly 55 000 events with visible K_S^0 decays, $K_S^0 \rightarrow \pi^+\pi^-$ and $K_S^0 \rightarrow \pi^0\pi^0$, in the full fiducial volume of the bubble chamber. These K_S^0 decays could be associated with primary $K^+\text{Xe}$ vertices with various multiplicities of secondary particles. Finally, events with a single proton and $K_S^0 \rightarrow \pi^+\pi^-$ in the final state were selected as candidates for the charge-exchange reaction $K^+n \rightarrow K^0p$ on a bound neutron. The selected events are then fully measured and reconstructed in space. These measurements are still in progress. The quality of the data is best reflected by experimental resolution on effective mass of the pK^0 system, estimated as $\sigma_m \simeq 3.5$ MeV by error propagation for observed events.

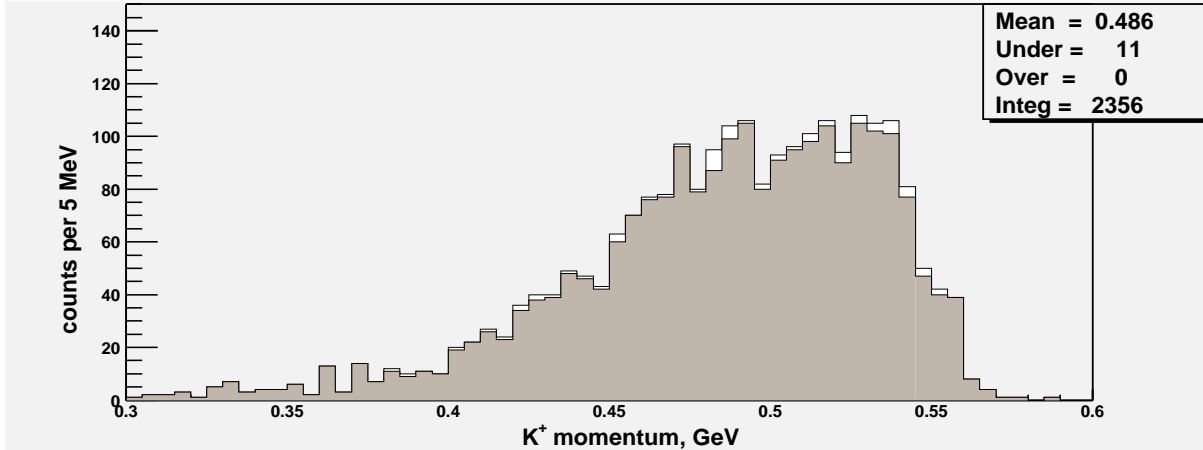


Figure 1: The incident K^+ momentum for measured events of the reaction $K^+\text{Xe} \rightarrow K^0p\text{Xe}'$. The shaded histogram results from restricting the K_S^0 proper lifetime: $\tau < 3\tau_0$.

At present, measurements have been restricted to the region $L_K > 520$ mm, where L_K is the length of the K^+ path in liquid Xenon before the collision. (Note that there is no one-to-one correspondence between L_K and K^+ momentum, because the original beam momentum varied by some ± 20 MeV in different exposures.) Shown in Fig. 1 is the lab momentum of the incident K^+ for all measured events with K_S^0 and proton momenta above 160 and 170 MeV, respectively (instrumental thresholds). Note that the statistics of the charge-exchange reaction has been increased by some 11% as compared to [7], and that newly measured events are mostly in the high-momentum region. For further rejection of K_S^0 mesons that may have scattered by small angles in liquid Xenon

but passed the pointback criteria, we then apply the selection $\tau < 3\tau_0$ where τ is the K_S^0 measured proper lifetime and τ_0 is its tabulated mean value.

Figure 2 shows the distributions of measured pK_S^0 events with $\tau < 3\tau_0$ in the following kinematic variables :

- laboratory momenta of the K_S^0 and proton ;
- in the pK_S^0 rest frame, the K_S^0 and K^+ angles with respect to the pK_S^0 boost from the laboratory frame, denoted as $\Theta^*(K_S^0)$ and $\Theta^*(K^+)$;
- in the laboratory frame, the longitudinal momentum of the pK_S^0 system as a whole, $p_L(pK_S^0)$;
- the effective target mass $m_{\text{targ}}^{\text{eff}}$, computed assuming binary kinematics.

Also shown are corresponding distributions of simulated events prior to any proton or K_S^0 rescattering in nuclear matter,¹ that have been normalized to the number of measured events. The K_S^0 and proton momenta are seen to be reduced by rescattering, see Figs. 2a and 2b. The effect is stronger for protons in agreement with the assumption that the free path in nuclear matter is bigger for kaons than for protons [19]. Likewise, the K_S^0 tends to travel in the forward hemisphere in the pK_S^0 frame, see Fig. 2c, because rescattering in nuclear matter is more probable for protons than for kaons. The K^+ travels exclusively in the forward direction $\cos \Theta^*(K^+) > 0$ for simulated events, see Fig. 2d, but also in the backward hemisphere for live events. For the pK_S^0 longitudinal momentum plotted in Fig. 2e, the simulation predicts that unrescattered events should populate the region $p_L > 0$, whereas the live events extend down to some -300 MeV. The distribution of the effective target mass $m_{\text{targ}}^{\text{eff}}$ is much broader for the live data than for simulated events,

¹The non-resonant charge-exchange reaction $K^+n \rightarrow K^0p$ in nuclear environment is simulated using a simple Monte-Carlo procedure. The total cross-section as a function of collision energy is parametrized using the existing data [18], and the angular distribution in the pK_S^0 rest frame is assumed to be isotropic. The total energy of a bound neutron is parametrized as $E_n = m_n - \epsilon$ where m_n is the mass of a free neutron and $\epsilon \simeq 22$ MeV is the mean binding energy for nucleons in the Xenon nucleus. For the same nucleus, we use a realistic form of the Fermi-momentum distribution with maximum near 160 MeV/c. Pauli blocking for secondary protons is approximated by the cut $p_p > 170$ MeV on proton momentum. The flux of incident K^+ mesons as a function of K^+ momentum at collision point is inferred from the observed distribution of K^+ range in Xenon before interaction or decay, see [5]. The experimental uncertainties and measurements errors are included in the simulation. Rescattering in the nucleus is not accounted for.

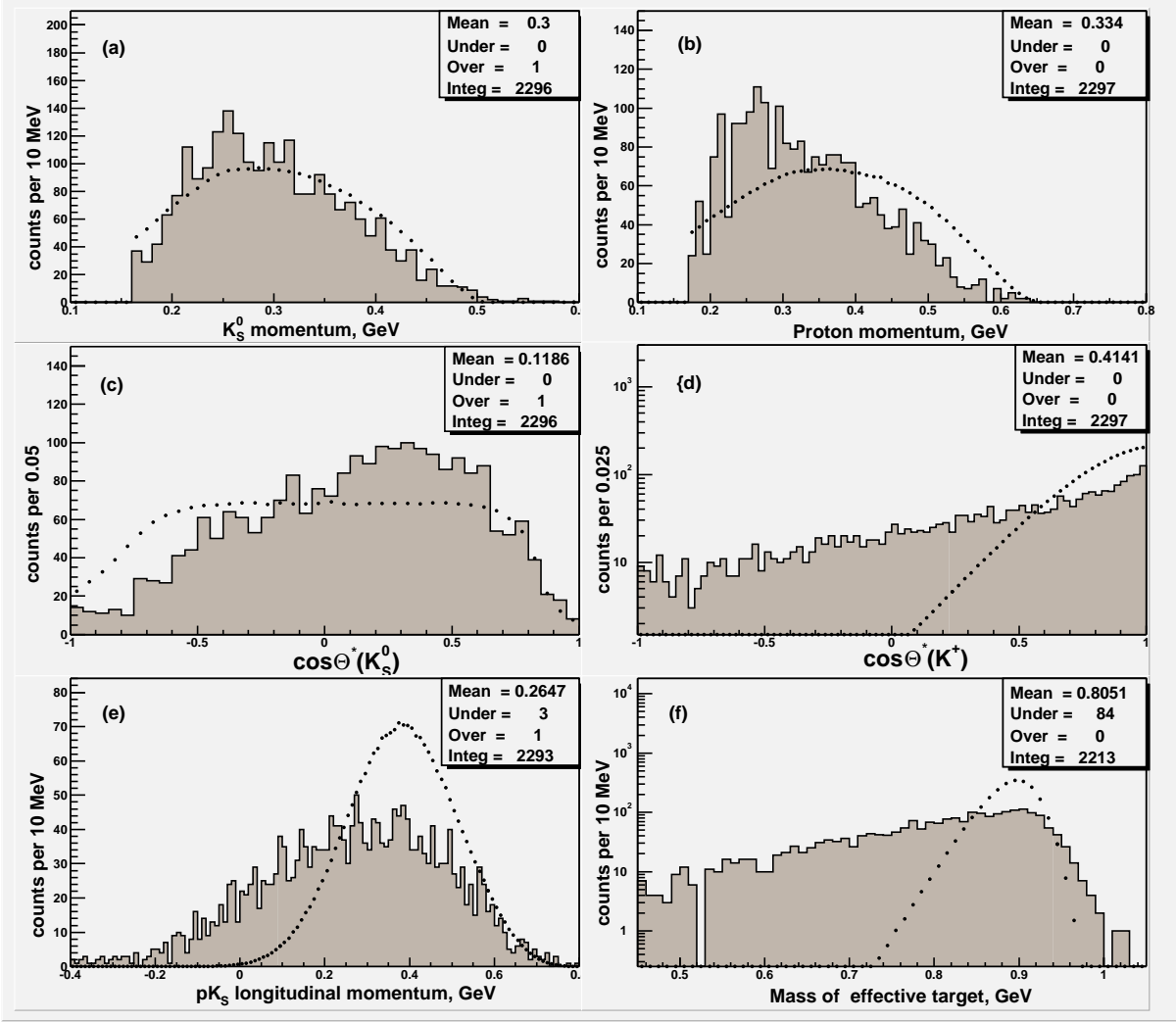


Figure 2: Laboratory momenta of the K_S^0 (a) and proton (b), the cosines of the K_S^0 angle (c) and of the K^+ angle (d) in the pK_S^0 rest frame, the longitudinal momentum of the pK_S^0 system in the lab frame (e), and the effective target mass $m_{\text{targ}}^{\text{eff}}$ (f). The dotted histograms are the corresponding distributions of simulated events prior to any proton or K_S^0 rescattering in nuclear matter, that have been normalized to the number of measured events.

see Fig. 2f, because rescattering disrupts the two-body kinematics of the reaction $K^+n \rightarrow K^0p$.

Compared in Fig. 3 are the distributions of two interrelated variables: the effective mass of the detected pK_S^0 system, $m(pK_S^0)$, and the center-of-mass energy of the K^+n collision assuming a stationary free neutron as the target, \sqrt{s} . That the $m(pK_S^0)$ spectrum is broader than the \sqrt{s} distribution is due to Fermi motion of the target neutron, as well as to rescattering of the secondary proton and K^0 in nuclear medium that distorts the

mass of the originally formed pK_S^0 system.

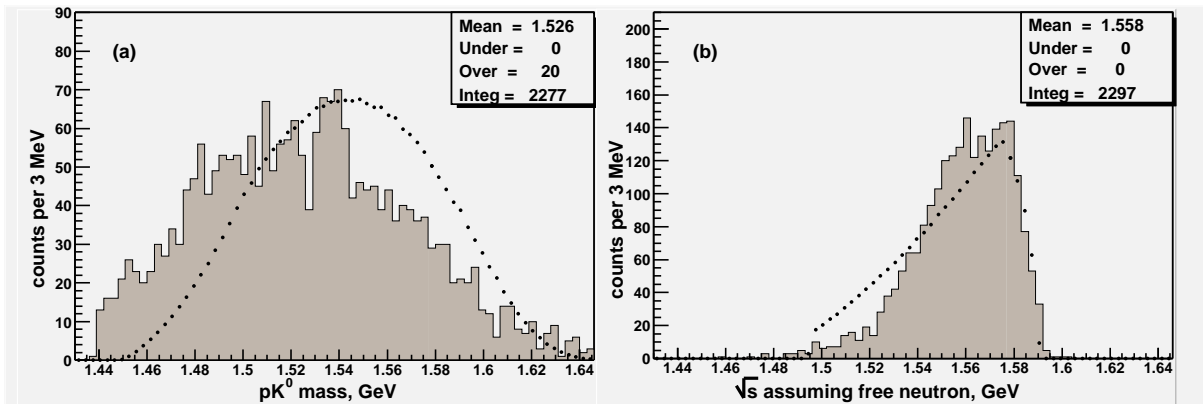


Figure 3: The effective mass of the detected pK_S^0 system (a) and the center-of-mass energy of the K^+n collision assuming a stationary free neutron as the target (b). The dotted histograms depict the distributions of simulated unscattered events normalized to the number of measured events.

Qualitatively, K^+ collisions with bound and free neutrons should form pK_S^0 systems with similar effective masses (prior to proton and K_S^0 rescattering). The mass difference $\Delta m = m(pK_S^0) - \sqrt{s}$ and the asymmetry $A_m = (m(pK_S^0) - \sqrt{s}) / (m(pK_S^0) + \sqrt{s})$ are plotted in Fig. 4 for live and simulated events of the charge-exchange reaction. For simulated events, the “original” value of the pK_S^0 mass prior to any rescattering is substituted. The observed Δm and A_m distributions are seen to extend to negative values far in excess of the smearing expected from neutron binding in the Xe nucleus. In order to suppress rescattered events, we use the selection $|A_m| < 0.015$ suggested by the simulation. The effect of this selection on the distribution of $\cos \Theta^*(K_S^0)$, the cosine of the K_S^0 emission angle in the pK_S^0 rest frame, is shown in Fig. 5a. By suppressing rescatterings, the selection $|A_m| < 0.015$ is seen to render the latter distribution more uniform. On the other hand, this selection brings the $m_{\text{targ}}^{\text{eff}}$ distribution to better agreement with the mass of a bound neutron, see Fig. 5b.

The $m(pK_S^0)$ distribution under the selection $|A_m| < 0.015$ shows an enhancement near 1538 MeV whose width is consistent with instrumental smearing alone, see Fig. 6. In the fit of this $m(pK_S^0)$ spectrum to a Gaussian on top of a third-order polynomial, the width of the Gaussian is constrained to $\sigma = 3.5$ MeV as estimated for a zero-width resonance by propagating measurement errors for observed pK_S^0 pairs. This fit returns nearly 100 events above background. In order to further reduce the background from rescatterings, an additional selection is used: $\Theta_K < 100^\circ$ and $\Theta_p < 100^\circ$ for polar angles of the K_S

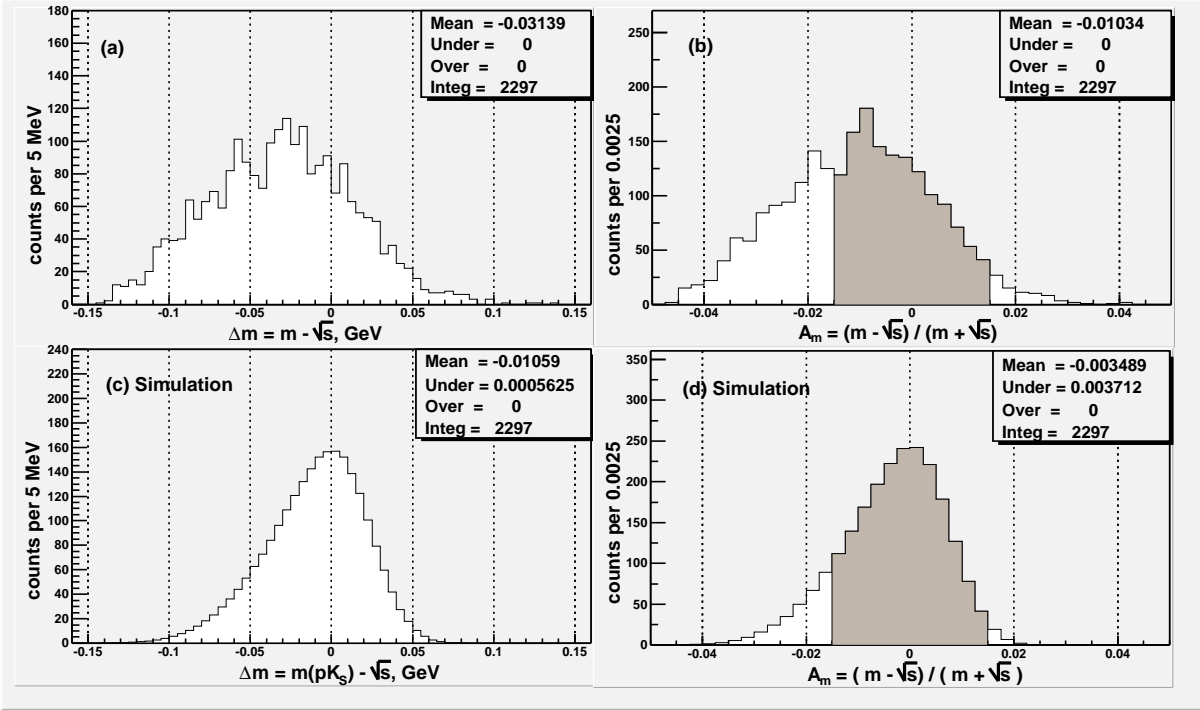


Figure 4: The mass difference $\Delta m = m - \sqrt{s}$ (a) and the asymmetry $A_m = (m - \sqrt{s}) / (m + \sqrt{s})$ (b) for observed events. Corresponding distributions of simulated events are shown in (c) and (d). Shaded areas in (b) and (d) are for $|A_m| < 0.015$.

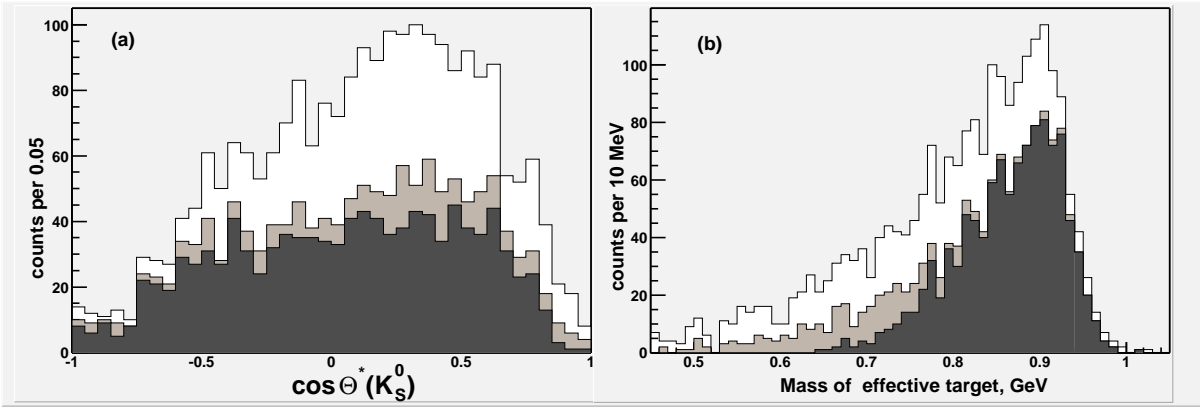


Figure 5: The cosine of the K_S^0 emission angle in the pK_S^0 frame (a) and the effective target mass assuming binary kinematics (b). Shaded histograms are for the selection $|A_m| < 0.015$. Dark histograms result from an additional selection $p_L(pK_S^0) > 80$ MeV.

and proton as in [7], or $p_L(pK_S^0) > 80$ MeV as suggested by Fig. 2e, or $\cos \Theta^*(K^+) > 0.2$ as suggested by Fig. 2d. Each additional selection further flattens the $\cos \Theta_{\text{cm}}$ distribution and suppresses the downward tail of the $m_{\text{targ}}^{\text{eff}}$ distribution (for $p_L > 80$ MeV, this is illustrated in Fig. 5). On the other hand, each selection further emphasizes the pK_S^0 peak near

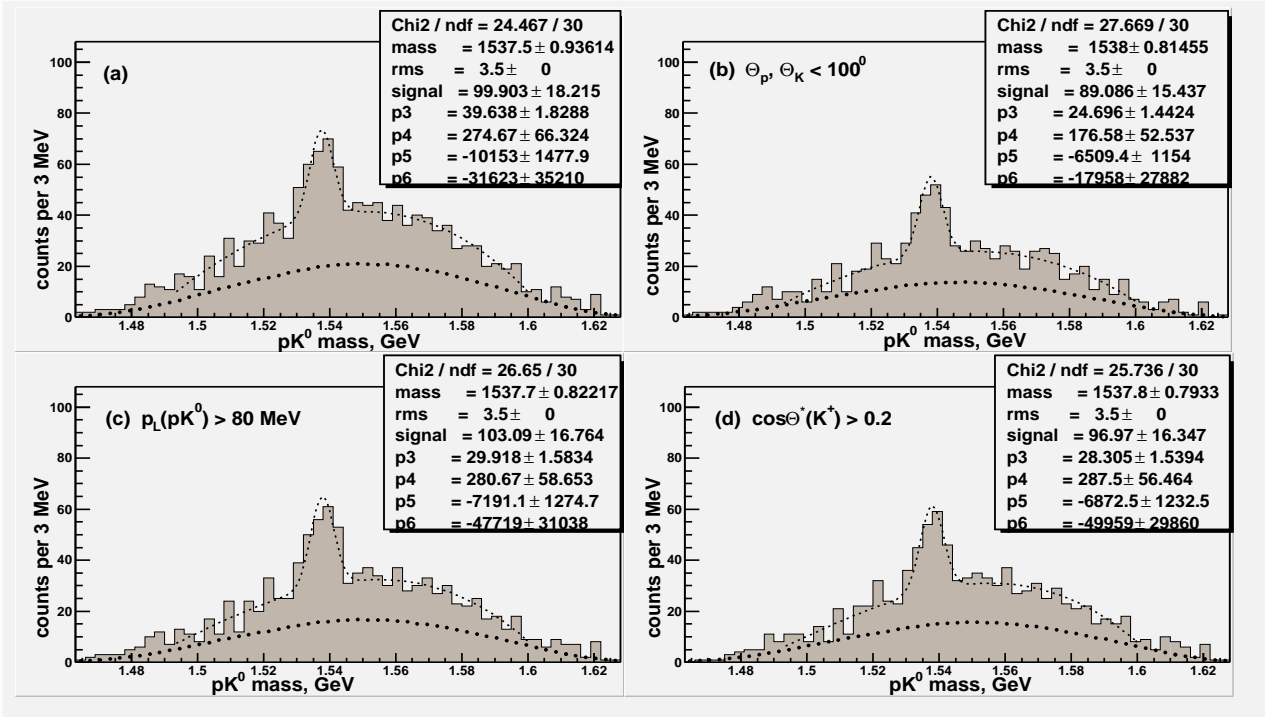


Figure 6: Effective mass of the pK_S^0 system upon applying the selection $|A_m| < 0.015$ (a). An additional selection is $\Theta_K < 100^\circ$ and $\Theta_p < 100^\circ$ in (b), $p_L(pK_S^0) > 80 \text{ MeV}$ in (c), and $\cos\Theta^*(K^+) > 0.2$ in (d). Depicted by dotted curves are fits to a Gaussian on top of a third-order polynomial. The width of the Gaussian has been constrained to $\sigma = 3.5 \text{ MeV}$. The solid dots are simulated distributions assuming no rescatterings, each normalized to the corresponding experimental distribution by area outside the peak region $1529 < m(pK_S^0) < 1547 \text{ MeV}$. The simulated mass spectra have been scaled by a factor of 0.5 in order to avoid confusion with the fitting function.

1538 MeV, see Figs. 6b, 6c, and 6d. The statistical significance of the signal reaches some 8σ (6σ) when estimated as S/\sqrt{B} ($S/\sqrt{B+S}$). Also shown in Fig. 6 are the simulated distributions of the pK_S^0 effective mass prior to any rescatterings under similar selections. Each of these has been normalized to the corresponding experimental distribution by area outside the peak region $1529 < m(pK_S^0) < 1547 \text{ MeV}$. That peak position is very close to the maximum of the non-resonant background may lead to overestimating the signal. So we additionally fit the difference between the experimental and simulated distributions, see Fig. 7. The fits of subtracted mass spectra return virtually the same signals as in Fig. 6, suggesting that the fitting procedure is robust.

In ref. [7] where the selections $\Theta_K < 100^\circ$ and $\Theta_p < 100^\circ$ were used, we argued that the bulk of the Θ^+ signal should arise from incident K^+ mesons with momenta in a restricted interval. Plotted in Fig. 8 is the pK_S^0 effective mass under the selections

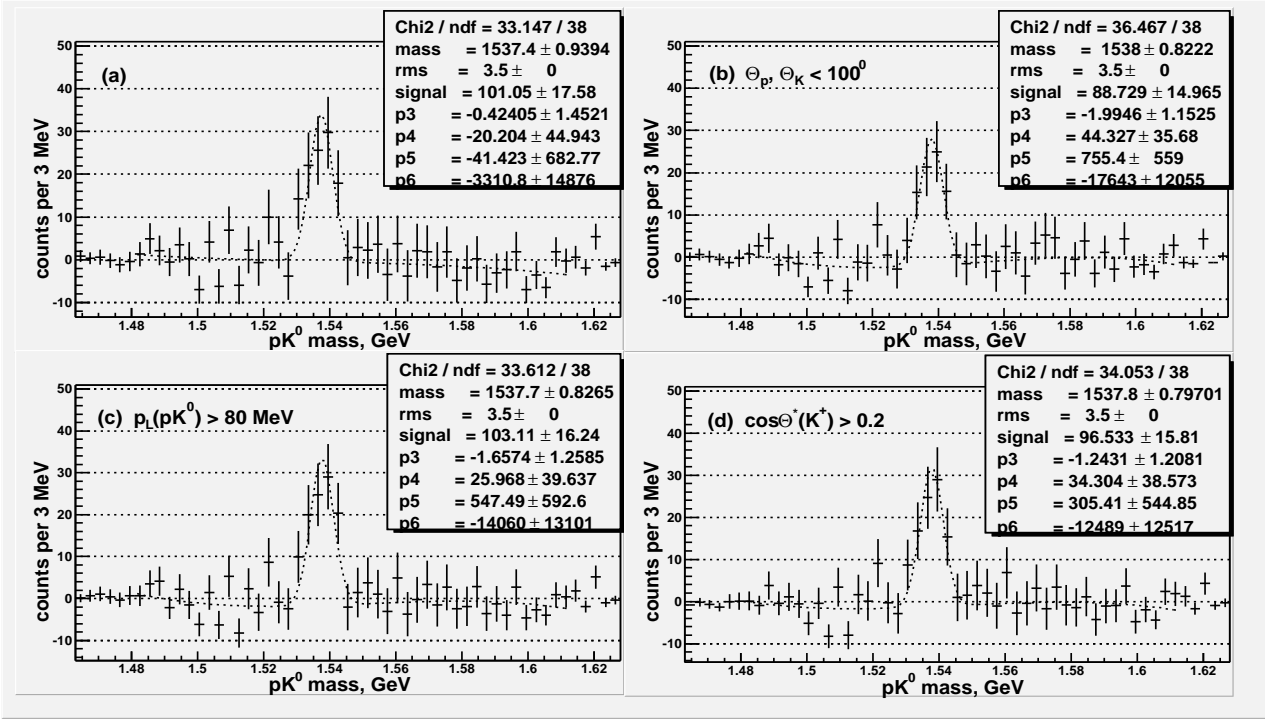


Figure 7: The difference between the experimental and simulated spectra of the pK_S^0 effective mass, as shown in Fig. 6.

as in Fig. 6b plus the additional selection $445 < p(K^+) < 525$ MeV as in [7]. This is separately done for the complete sample of the charge-exchange reaction and for the part of the sample analyzed in [7]. The signal in Fig. 8b is virtually the same as that reported in [7]. Combining the selections $|A_m| < 0.015$ and $445 < p(K^+) < 525$ MeV is of course a redundant procedure used only for comparing with our previous results. That the selection $|A_m| < 0.015$ is not tuned to any particular value of the pK_S^0 effective mass is its obvious advantage.

Intrinsic width of a resonance formed in an s -channel reaction like $K^+n \rightarrow K^0p$ can be estimated by comparing the signal magnitude with the level of non-resonant background under the peak, see *e.g.* [13]. However, this method cannot be directly applied to K^+ collisions with heavy nuclei because of secondary interactions of the K^0 and proton in nuclear medium. That is, the non-resonant background under the peak is an unknown mixture of unscattered and rescattered events, whereas a true signal should consist of unscattered events only. As soon as the Θ^+ decay width is ~ 1 MeV or less, the peak will not be depleted by the K_S^0 and proton rescatterings because the bulk of produced Θ^+ baryons will decay upon leaving the nucleus. The corresponding “rescattering-free” back-

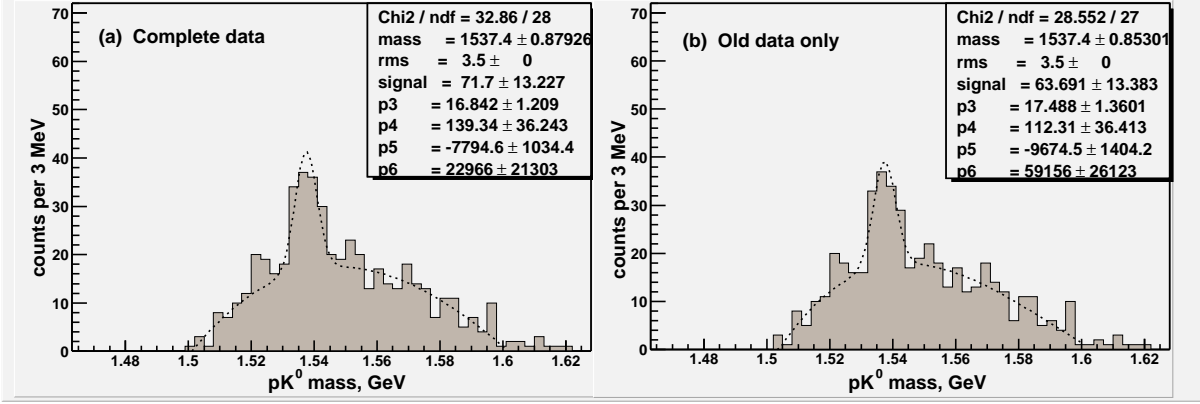


Figure 8: The pK_S^0 effective mass under the selections as in Fig. 6b ($|A_m| < 0.015$, $\Theta_K < 100^\circ$, and $\Theta_p < 100^\circ$) plus the additional selection $445 < p(K^+) < 525$ MeV. The data for the complete sample of the charge-exchange reaction and for the part of the sample analyzed in [7] are shown in (a) and (b), respectively.

ground can only be estimated by simulating the effective mass of the originally produced K_S^0 and proton prior to any rescatterings, $m_0(pK_S^0)$.

For the simulated charge-exchange collisions $K^+n \rightarrow K^0p$ on a bound neutron in the bubble chamber DIANA, the K^+ momentum at collision point and the “undistorted” mass $m_0(pK_S^0)$ are plotted in Fig. 9. The K_S^0 lab momentum is restricted to $p_K > 140$ MeV which is the (effective) threshold for detecting $K_S^0 \rightarrow \pi^+\pi^-$ decays in the scan. The upper histograms are for all collisions in the full fiducial volume, *i.e.*, over the full range of L_K —the K^+ track length in Xenon before the collision. The shaded area of the K^+ momentum distribution corresponds to the restricted fiducial volume $L_K > 520$ mm where throughput measurements were done. The absolute normalization of the simulated distributions of Fig. 9 is based on the scanning information. In the region $L_K > 520$ mm, the scan found 7900 ± 500 events with a $K_S^0 \rightarrow \pi^+\pi^-$ candidate in the final state. Of these events, $(60 \pm 7)\%$ are estimated to survive upon rejecting K_S^0 mesons with $L < 2.5$ mm, protons and K_S^0 mesons that have reinteracted in liquid Xenon, and unmeasurable events. The resultant number of events, 4740 ± 630 , is then used for absolute normalization of the simulated K^+ -momentum distribution for $L_K > 520$ mm, see the shaded area in Fig. 9a. The distribution of the same events in $m_0(pK_S^0)$ is shown by the corresponding shaded histogram in Fig. 9b. And finally, the absolute level of the non-resonant background can be estimated upon applying the aforementioned selections to simulated events: $p_K > 160$ MeV, $p_p > 170$ MeV, $\tau < 3\tau_0$, and $|A_m| < 0.015$. The resultant $m_0(pK_S^0)$ distribution, depicted by the dark-shaded histogram in Fig. 9b, features 705 ± 94 events in the mass

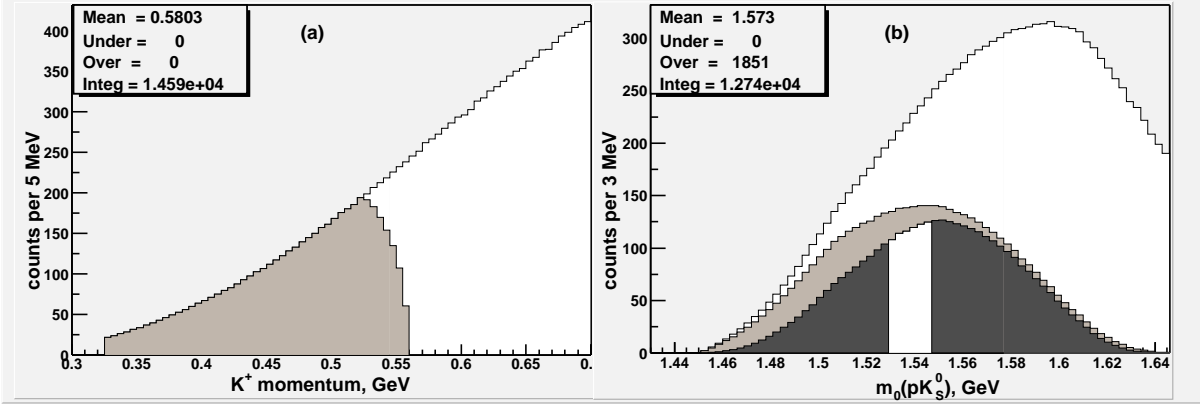


Figure 9: The K^+ momentum (a) and the “undistorted” mass $m_0(pK_S^0)$ (b) for simulated charge-exchange collisions $K^+n \rightarrow K^0p$ in the bubble chamber DIANA. The upper histograms are for all collisions with $p_K > 140$ MeV in the full fiducial volume. The shaded histograms are for K^+ track lengths $L_K > 520$ mm (the region of throughput measurements). The dark-shaded histogram in (b) results from the adopted selections $p_K > 160$ MeV, $p_p > 170$ MeV, $\tau < 3\tau_0$, and $|A_m| < 0.015$. The open-white corridor in the latter histogram depicts the mass region $1529 < m_0(pK_S^0) < 1547$ MeV. The normalization is explained in the text.

region $1529 < m_0(pK_S^0) < 1547$ MeV.

Using the observed signal and simulated background as input and assuming $J = 1/2$, we then estimate the intrinsic width of the pK^0 resonance as [13]

$$\Gamma = \frac{N^{\text{peak}}}{N^{\text{bkgd}}} \times \frac{\sigma^{\text{CE}}}{107\text{mb}} \times \frac{\Delta m}{B_i B_f},$$

where N^{peak} and N^{bkgd} are the numbers of events in the peak and in the background under the peak, $\sigma^{\text{CE}} = 4.1 \pm 0.3$ mb is the measured cross section of the charge-exchange reaction $K^+n \rightarrow K^0p$ [18], B_i and B_f are the branching fractions for the initial and final states ($B_i = B_f = 1/2$ for either $I = 0$ and $I = 1$), and Δm is the $m(pK_S^0)$ interval under the peak that is populated by N^{bkgd} background events. Selecting a mass interval $1529 < m(pK^0) < 1547$ MeV and substituting $N^{\text{peak}} = 99.9 \pm 18.2$ events from Fig. 6a and $N^{\text{bkgd}} = 705 \pm 94$ events from Fig. 9b, we obtain $\Gamma = 0.39 \pm 0.10$ MeV where the error does not include the systematic uncertainties of the simulation procedure. A systematic shift of up to +20% may result from taking into account the sequential reaction $K^+N \rightarrow K^+N$, $K^+n \rightarrow K^0p$ [20]. The value of Γ derived in this analysis is consistent with our earlier estimate [7] and with the upper limit set by BELLE [11].

To conclude, we have reanalyzed the DIANA data on the charge-exchange reaction

$K^+Xe \rightarrow K^0pXe'$ using increased statistics and updated selections. We have obtained new strong evidence for formation of a pentaquark baryon with positive strangeness in the charge-exchange reaction $K^+n \rightarrow K^0p$ on a bound neutron. The statistical significance of the signal reaches some 8σ (6σ) when estimated as S/\sqrt{B} ($S/\sqrt{B+S}$). The mass and intrinsic width of the Θ^+ baryon are measured as $m = 1538 \pm 2$ MeV and $\Gamma = 0.39 \pm 0.10$ MeV.

We wish to thank Ya. I. Azimov, L. N. Bogdanova, and I. I. Strakovsky for useful comments. This work is supported by the Russian Foundation for Basic Research (grant 07-02-00684).

References

- [1] R.L. Jaffe, “Multi-quark hadrons”, Phys. Rev. D15, 267 (1977).
- [2] D. Diakonov, V. Petrov, and V. Polyakov, Z. Phys. A359, 305 (1997).
- [3] D. Diakonov and V. Petrov, Phys. Rev. D72, 074009 (2005);
 C. Lorce, Phys. Rev. D74, 054019 (2006);
 A.G. Oganesian, JETP Lett. 84, 409 (2006), arXiv:hep-ph/0605131;
 A.G. Oganesian, Int. J. Mod. Phys. A22, 2093 (2007), arXiv:hep-ph/0608031;
 Cedric Lorce, arXiv:0705.1505 [hep-ph];
 Hyun-Chul Kim, Tim Ledwig, and Klaus Goeke, Mod. Phys. Lett. A23, 2238 (2008),
 arXiv:0802.2368 [hep-ph];
 Hyun-Chul Kim *et al.*, arXiv:0905.4228 [hep-ph].
- [4] T. Nakano *et al.* (LEPS Coll.), Phys. Rev. Lett. 91, 012002 (2003).
- [5] V. V. Barmin *et al.* (DIANA Coll.), Yad. Fiz. 66, 1763 (2003) and Phys. At. Nucl. 66, 1715 (2003).
- [6] T. Nakano *et al.* (LEPS Coll.), Phys. Rev. C79, 025210 (2009), arXiv:0812.1035 [nucl-ex].
- [7] V.V. Barmin *et al.* (DIANA Coll.), Yad. Fiz. 70, 39 (2007) and Phys. At. Nucl. 70, 35 (2007), arXiv:hep-ex/0603017.
- [8] Volker D. Burkert, Int. J. Mod. Phys. A21, 1764 (2006), arXiv:hep-ph/0510309.

- [9] M.V. Danilov and R.V. Mizuk, Phys. Atom. Nucl. 71, 605 (2008), arXiv:0704.3531 [hep-ex].
- [10] Dmitri Diakonov, AIP Conf. Proc. 892, 258 (2007), arXiv:hep-ph/0610166.
- [11] R. Mizuk *et al.* (BELLE Coll.), Phys. Lett. B632, 173 (2006).
- [12] R.A. Arndt, I.I. Strakovsky, and R.L. Workman, Phys. Rev. C68, 042201 (2003), arXiv:nucl-th/0308012.
- [13] R.N. Cahn and G.H. Trilling, Phys. Rev. D69, 011501 (2004), arXiv:hep-ph/0311245.
- [14] A. Sibirtsev *et al.*, Phys. Lett. B599, 230 (2004), arXiv:hep-ph/0405099.
- [15] W. Gibbs, Phys. Rev. C70, 045208 (2004), arXiv:nucl-th/0405024.
- [16] Ya.I. Azimov *et al.*, Eur. Phys. J. A26, 79 (2005), arXiv:hep-ph/0504022.
- [17] Norihito Muramatsu, talk at Workshop on Nuclear Physics at J-PARC, June 2007, Tokai, Japan.
- [18] U. Casadei *et al.*, CERN-HERA 75-1.
- [19] A. Sibirtsev *et al.*, Eur. Phys. J. A23, 491 (2005).
- [20] B. Sechi Zorn and G.T. Zorn, Phys. Rev. 120, 1898 (1960).